

1 Research Article

2
3 **Digital Urban Morphometrics: Automatic**
4 **Extraction and Assessment of**
5 **Morphological Properties of Buildings**
6

7 Cláudio Carneiro
8 *Geographical Information Systems*
9 *Laboratory*
10 *Ecole Polytechnique Fédérale de*
11 *Lausanne*

Eugenio Morello
Laboratorio di Simulazione Urbana
DIAP
Politecnico di Milano

12
13 Thomas Voegtli
14 *Institute of Photogrammetry and*
15 *Remote Sensing*
16 *University of Karlsruhe*

François Golay
Geographical Information Systems
Laboratory
Ecole Polytechnique Fédérale de
17 *Lausanne*

18
19 **Abstract**

20 The aim of this article is to present a method to calculate the morphological
21 properties of the built environment using LiDAR (light detection and ranging) data,
22 geographic information systems (GIS) data and three-dimensional (3D) models of
23 cities as a source of information. A hybrid approach that takes into account different
24 types of inputs and consequently evaluates the accuracy of each type of used data is
25 presented. This work is intended to give a first response to the lack of a compre-
26 hensive and accurate procedure that uses LiDAR data in order to automatically
27 derive precise morphological properties, such as volumes and surfaces (façades and
28 roofs) of buildings. The method was tested on two case-study areas in the Geneva
29 region with different characteristics, one in the old town along the Rhone River and
30 the other on the CERN campus. A statistical analysis that compares the results of the
31 computation with the 3D model of the built environment was used to validate the
32 results, complemented by significance statistical tests. Outcomes showed that the
33 proposed method to derive morphological properties can reach high levels of accu-
34 racy, thus enhancing the potential uses of LiDAR data for numerous applications,
35 typically for the assessment of the urban environmental quality (UEQ) at the city and
36

37 **Address for correspondence:** Cláudio Carneiro, EPFL–LASIG, Station 18, Bâtiment GC, CH-1015,
38 Lausanne, Switzerland. E-mail: claudio.carneiro@epfl.ch

1 district scale, such as the estimation of the potential deployment of renewable
2 energies in the built environment and the determination and monitoring of several
3 urban indicators.

5 1 Introduction

6
7 The aim of this work was to propose a method to calculate the morphological properties
8 of the built environment using light detection and ranging (LiDAR), geographic infor-
9 mation systems (GIS) data, and three-dimensional (3D) vectorial city models through
10 segmentation and image processing techniques. In particular, we explored different
11 methods suitable for the computation of volumes and surfaces (areas of façades and areas
12 of roofs) of buildings. Whereas image processing techniques offer widely tested methods
13 for the calculation of volumes, computation of surfaces is still an open topic when raster
14 images are used as the source information. Our hypothesis was that an automated
15 method (from raw LiDAR data through the reconstruction of a precise urban model to
16 the computation of morphological indicators) could dramatically increase the use of
17 LiDAR data, because it would accelerate the process of analysis with no need for
18 expensive 3D models.

19 Spatial data quality (SDQ) is an important subject in many decisions and analyses.
20 For centuries geographers and cartographers have been concerned with the collection,
21 storage, analysis, and visualization of two-dimensional (2D) spatial data. Since the
22 1960s, with the emergence of GIS, there has been a rising availability, exchange, and use
23 of 2D spatial data. Moreover, in the past decade, new types of 3D spatial data have
24 arisen, such as LiDAR, increasing considerably the number of sources available and
25 potential applications, for example, as presented in this article, for the extraction of
26 morphological properties of buildings.

27 According to Aalders (2002) and Devillers et al. (2005), SDQ can be described using
28 5–11 elements. One of them is the description of spatial/positional accuracy of a given
29 dataset, which will be the main focus of this article in relation with SDQ. Thus, for each
30 of the three morphological properties of buildings (volume, area of roofs, and area of
31 façades) under analysis, the set of data derived from LiDAR data from which the
32 spatial/positional accuracy has to be calculated is called the test data set, and the set of
33 data calculated from a real 3D vectorial city model is called the reference dataset. Section
34 5 of this article assesses the performed calculations by applying a statistical analysis and
35 significance tests between the different methods and data used.

36 Nowadays, airborne LiDAR sensors allow scanning large urban areas with an
37 increased resolution. Therefore, the increased accuracy of remote sensing detection
38 technologies, the better availability, and the decreasing price for acquiring this type of
39 data, render it very attractive for local scale applications, such as the urban environment.
40 Therefore, the need to implement procedures to make LiDAR data useful for urban
41 studies is a topic that was investigated in the past decade, but precise methods that can
42 analyse these data are still lacking. For instance, applications are very promising in urban
43 studies, where there is an increasing awareness of the use of 3D digital information for
44 the analysis and the description of the properties of the built environment.

45 Researchers in urban studies are more and more concerned about the improvement
46 of the quality of life in our cities, where more than half of the world's population resides.
47 Towards a better understanding of the urban environmental quality (UEQ), several

1 indicators and measurements were proposed in past years to analyse and compare
2 built-up areas worldwide, involving cross-disciplinary competences in urban design and
3 planning, health, ecology and transportation, among others. One set of those indicators
4 deals directly with the measurement of the urban form, aiming at quantifying the role of
5 the built fabric in assessing the environmental performance of cities and revealing
6 structural features of different built-up areas. For instance, we refer to the term “urban
7 morphometrics,” which was deliberately transferred from other disciplines. In fact,
8 morphometrics studies the variation and change in the form of objects, and is widely used
9 in biology, zoology, and medicine, whereby different methods to extract data from shapes
10 are investigated.

12 2 The Calculation of Morphological Indicators: Related Work

13
14 This work combined two research streams that developed during the past 15 years: the
15 use of digital image processing (DIP) techniques to process raster images of cities and
16 extract useful information, and the techniques that apply LiDAR data in urban studies
17 from a 3D GIS viewpoint.

18 Pioneers in the use of image processing techniques for the analysis of environmental
19 indicators and morphology of digital urban models were a group of researchers at the
20 Martin Centre, University of Cambridge (Ratti and Richens 2004). This research was
21 further improved at the Senseable City Lab at the Massachusetts Institute of Technology,
22 who proposed applications for assessing the solar admittance of the urban fabric through
23 solar envelopes (Morello and Ratti 2009a) and the visual perception of the urban open
24 spaces through the use of 2D and 3D isovists (Morello and Ratti 2009b).

25 Until now some authors have introduced the applicability of LiDAR data in urban
26 studies, but did not delve deeply into the calculation and validation of some morpho-
27 logical indicators (Carneiro et al. 2008, 2009a, b). In this study we introduce a novel
28 method for the automatic extraction and assessment of morphological properties of
29 buildings using different data sources, as presented in the next sections of this article.

30 Previous literature on interpolation of LiDAR point clouds is vast. The advantages
31 and disadvantages of several interpolation methods, such as triangle-based linear inter-
32 polation, nearest neighborhood interpolation, and kriging interpolation were presented
33 by Zinger et al. (2002). The most accurate surfaces are created using a grid with a
34 sampling size that relates as close as possible to the LiDAR point density during the
35 acquisition phase (Behan 2000). A method for constructing a 2.5D urban surface model
36 (2.5-DUSM) incorporating the geographical relief, based on LiDAR and GIS buildings
37 data, was proposed by Osaragi and Otani (2007).

38 Many authors have studied the segmentation procedure for LiDAR data. For
39 example, Vosselmann and Dijkman (2001) used 3D Hough transform to detect planes in
40 LiDAR data and Hofmann et al. (2003) made a comparison between 2D and 3D Hough
41 transform for detecting building planes in LiDAR data. An algorithm for the automated
42 delineation of roof planes from LiDAR data was proposed by Rottensteiner et al. (2005).

43 A 3D urban GIS including the reconstruction of buildings from laser altimeter and
44 2D map data was proposed by Haala et al. (1998). The advantages related to the
45 integration of these two types of data sources were analyzed by Vosselmann (2002).

46 A first method that allows the derivation of morphological properties of city blocks
47 using an urban landscape model, constructed from a large LiDAR dataset, was presented

1 by Yoshida and Omae (2005). Using different topographical data, Koomen and Bação
2 (2005) presented a new methodology that describes the density of urban systems and
3 allows the quantification of the urban volume.

4 5 **3 Method**

6 *3.1 Dataflow Process*

7 The process for structuring the proposed method was based on four major steps, as
8 represented in the dataflow of Figure 1: (1) the classification and segmentation procedure
9 for laser scanning data; (2) the construction of the normalized 2.5 Digital Urban Surface
10 Model (n2.5-DUSM) of buildings and the n2.5-DUSM of roofs; (3) the creation of the
11 different grid masks used; (4) the programming of scripts, using segmentation and DIP
12 techniques, allowing calculation of the output results. All these steps will be further
13 detailed and analyzed in the next three sections of this article.

14 The n2.5-DUSM of buildings and the n2.5-DUSM of roofs are image-based georef-
15 erenced information. They were constructed using a hybrid approach that integrates raw
16 LiDAR data and 2D vector digital maps, such as presented in the steps 1 and 2 of
17 Figure 1.

18 19 *3.2 Data Sources Used*

20 To test the method, two case-study areas are referred to. The first site (Figure 2, left-hand
21 image) is a selection of 18 buildings inside the campus of the European Organization for
22 Nuclear Research (CERN), more precisely the eastern area within the Swiss boundary.
23 Most of the buildings are characterized by simple geometry, but present different heights
24 and footprints; only some of them require particular attention in the computation
25 because they present very complex shapes, having multiple faces. The second site selected
26 for the analysis is a square near the Rhone River and the old town of Geneva, in
27 Switzerland, presented in Figure 2 (right-hand image): 45 different buildings with an
28 average height of 18.5 m are located at this site. The urban fabric is quite compact and
29 densely built. Buildings present many superstructures on roofs, are sufficiently separated
30 from each other, and do not present particular problems caused by the presence of
31 vegetation (for example trees touching the façades or roofs).

32 The following data were used:

- 33 1. *2D GIS building outlines.* For both case-study areas presented here the 2-D GIS
34 database of the Canton of Geneva was used to extract vectorial information about
35 building outlines, which were used to construct a more accurate n2.5-DUSM of
36 buildings, as introduced in Section 3.3.
- 37 2. *2D projection of 3D roof lines.* For both case-study areas presented here, the 2D
38 projection of 3D roof lines was used to extract vectorial information about building
39 roofs that was also used to construct a more accurate n2.5-DUSM of roofs, as
40 reported in Section 3.3.
- 41 3. *LiDAR data.* The LiDAR used for the construction of both normalized n2.5-DUSM
42 of buildings and n2.5-DUSM of roofs has a density of 4 points/m², a planimetric
43 accuracy of 20 cm and an altimetric accuracy of 15 cm. Due to the high accuracy of
44 LiDAR data, the use of detailed vectorial building outlines and vectorial roof lines

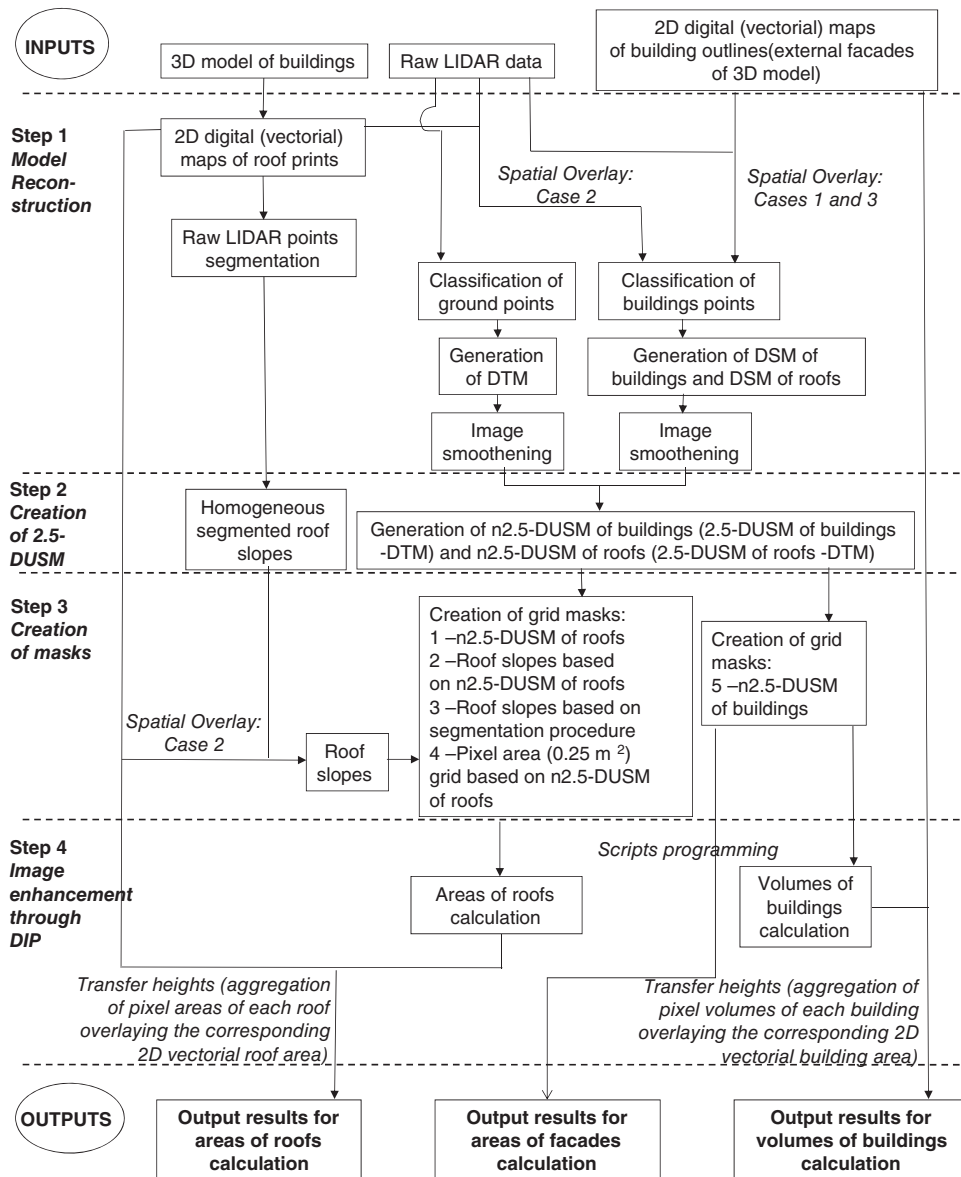


Figure 1 The dataflow process describing the method implemented to produce and analyze the n2.5-DUSM of buildings and the n2.5-DUSM of roofs

for classifying LiDAR points on buildings is crucial for the improvement of the n2.5-DUSM interpolation and construction, as introduced in Section 3.3.

4. *3-D city model*. An accurate 20–25 cm 3D vectorial city model of both case-study areas was used to extract information about the volume, areas of façades, and areas of roofs. It was reconstructed by combining: (1) a 2D vectorial information of the cadastral survey for the definition of the 3D building footprints; (2) a 3D stereoscopic model based on aerial images with a resolution of 16 cm, taken with a



Figure 2 The orthophotos of the two case-study areas. Left-hand image: the CERN campus; right-hand image: the site in the old town of Geneva, close to the Rhone River

Vexcel camera, for the semi-automatic digitalization of vectorial 3D building outlines. This information was used for assessment of the automatic extraction of morphological properties of buildings, as presented in Section 5.

3.3 Reconstruction of the Normalized 2.5-D Urban Surface Model of Buildings and the Normalized 2.5-D Urban Surface Model of Roofs

An n2.5-DUSM interpolated and reconstructed only from LiDAR data will have low geometrical accuracy for the analysis and extraction of indicators related to the morphology of buildings, primarily along its boundaries and zones of discontinuity. Thus, there should be great potential for the improvement of a building's geometry through:

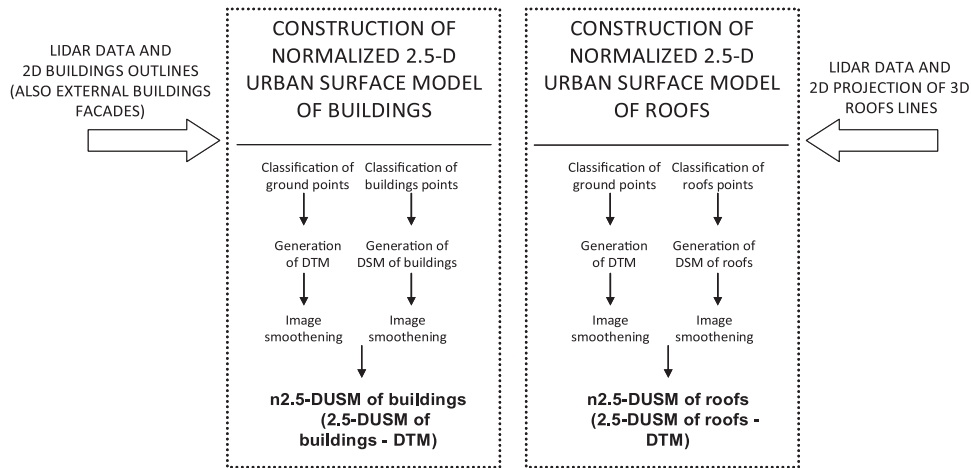
- The integration of other data sources, such as 2D GIS cadastral data for the calculation of volumes and areas of façades of buildings¹ and, if available, 2D projection of 3D roof lines for the calculation of areas of roofs.
- The use of non-direct interpolation techniques, undertaken independently of the terrain for each building.

A scheme that describes the structure of the procedure is shown in Figure 3, based on the method of Carneiro et al. (2009b). The method related to the construction of the n2.5-DUSM of roofs was similar to the one presented for the n2.5-DUSM of buildings. The n2.5-DUSM of buildings of the case-study area in the center of Geneva is represented in Figure 4.

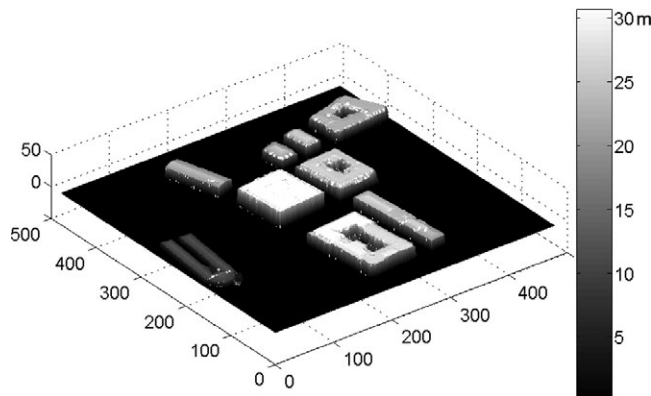
3.4 Calculation of Morphological Properties of Buildings using Segmentation and Image Processing Techniques

3.4.1 Overview

Once the model had been reconstructed, image processing operations were used in the MATLAB environment on a pixel basis to enable the calculation of morphological



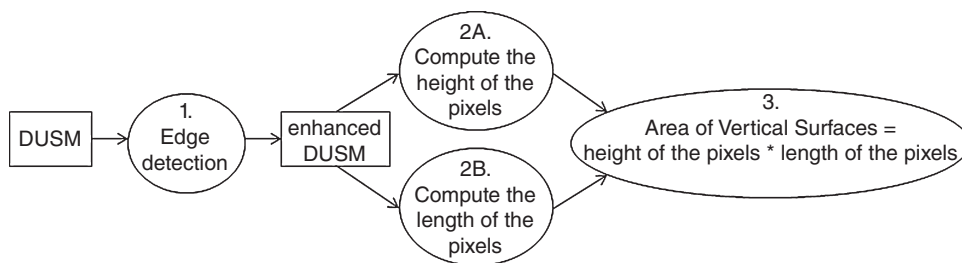
1 **Figure 3** Data used and general structure for the construction of the n2.5-DUSM of
2 buildings and the n2.5-DUSM of roofs



3
4 **Figure 4** The n2.5-DUSM of the case-study area at the center of Geneva

5
6 indicators. For instance, each building was imported as a single image, i.e. a 2D array
7 where the intensity value of each pixel corresponded to the height of the pixel in meters.
8 On each pixel belonging to the edges of the object a series of morphological operations
9 was performed and the results of those operations compared to the referred to 3D
10 model.

11 In order to compute the areas of the vertical surfaces of the object, first the edges of
12 the object must be detected; second, two separate procedures are required to establish the
13 height and length of each pixel, as shown in Figure 5. Both procedures require the
14 application of filters with the double aim of detecting the edges of the object and
15 assigning the proper values to them. Different types of morphological operations were
16 used in this work as follows: contraction and dilation operations on the external edges
17 of the object; the Canny filter² (Canny 1986) and other operations to average the value
18 of the pixels considering various types of structuring elements.³



1 **Figure 5** Structure of the procedure related to the calculation of vertical areas of
2 façades

3
4 **3.4.2 The enhancement of the normalized 2.5-DUSM of buildings and the**
5 **normalized 2.5-DUSM of roofs**

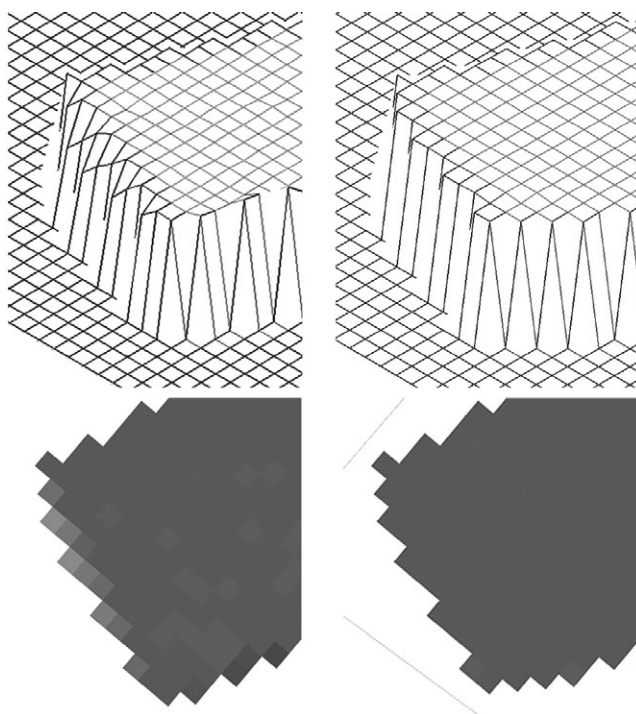
6 The first set of operations to detect the edges of the object was performed in order to
7 reduce the noise on the DUSM. In particular, the morphological operations to enhance
8 the model were performed in three steps presented below.

- 9
- 10 1. The enhancement on both the original n2.5-DUSM of buildings and n2.5-DUSM of
11 roofs obtained by combining operations of contraction and dilation on the perimeter
12 of the object alone. In this routine a 3 pixels by 3 pixels neighborhood with a
13 diamond shape was applied for both operations of contraction and dilation. For
14 instance, the contraction of the last contour of pixels on the perimeter of the object
15 allowed the reduction of the noise on the borders of buildings caused by the
16 interpolation of raw LiDAR data. The second step was the dilation of the new
17 boundary (emerging from the operation of contraction). This action averaged the
18 values on the pixels of the perimeter on their original location (refer to Figure 6).
19 Both the original n2.5-DUSM of buildings and n2.5-DUSM of roofs and the respec-
20 tive enhanced models were used for the computation of morphological indicators. A
21 comparison of results is presented in Section 4.
 - 22 2. The second set of morphological operations aimed to refine the boundaries of the
23 object and was performed applying again a contraction and dilation of the external
24 boundaries of the object through different flat structural elements of different size
25 and shape. The Canny filter was applied on these latter detected external edges of the
26 object.
 - 27 3. A new enhancement with diamond filters on the enhanced model could be performed
28 as presented in point 1. This step was necessary to also detect internal vertical
29 surfaces, as opposed to step 2 where only external ones are marked.

30 **3.4.3 Segmentation of planar roof areas**

31 The segmentation of roof planes could, in principle, be performed directly on the laser
32 point cloud, but the point cloud was rasterized (in this case onto a grid size of 0.5 m) in
33 a first step by a region growing algorithm for easier and faster determination.

34 This starts at the so-called seed area, a local neighborhood of a point (e.g. 3 pixels
35 by 3 pixels) where the laser points fulfill user defined conditions. In this case all points of



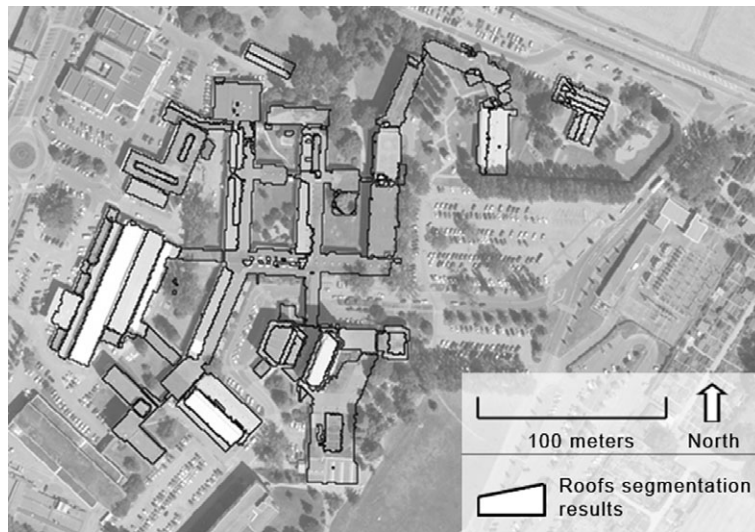
1 **Figure 6** Enhancement of a portion of a DUSM obtained by applying a set of image
2 processing morphological operations (contraction and dilation on the edges of the
3 object). Left-hand images: the original DUSM represented as an isometric view (above)
4 and as a top view (below); right-hand images: the enhanced object is characterized by
5 sharper edges

6
7 the seed area must lie in the same plane (initial plane) with only small acceptable
8 deviations (e.g. due to data noise), i.e. the point coordinates must fulfill the mathematical
9 equation of a plane.

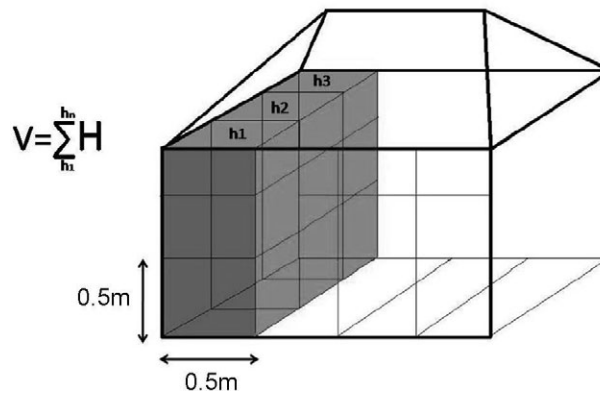
10 After determination of the initial plane the region growing algorithm iteratively
11 analyses the adjacent points. A point is added to this plane if it fulfills a so-called
12 *homogeneity condition*, by means of the orthogonal distance of the point to the current
13 plane. The point is accepted and integrated if this distance is small enough to fulfill a
14 probability condition and the plane parameters are recalculated by an adjustment pro-
15 cedure. If no new adjacent points can be found the region growing stops, the plane area
16 (and its parameters) are stored and subsequently masked out. Then the algorithm will
17 search for a new seed area and start segmenting a new plane until no new planes can be
18 found in the dataset.

19 This procedure was initially described by Quint and Landes (1996) and later
20 enhanced for application on LiDAR data by Vögtle and Steinle (2000). As proposed by
21 Lemp and Weidner (2005) the algorithm has also been applied using only last pulse laser
22 data, but results were not satisfying, especially along roof edges.

23 Figure 7 shows the result of the segmentation of roof planes for an area of the CERN
24 campus using all laser scanning pulse data.



1 **Figure 7** Segmentation of planar roof areas in the CERN test area (subset)

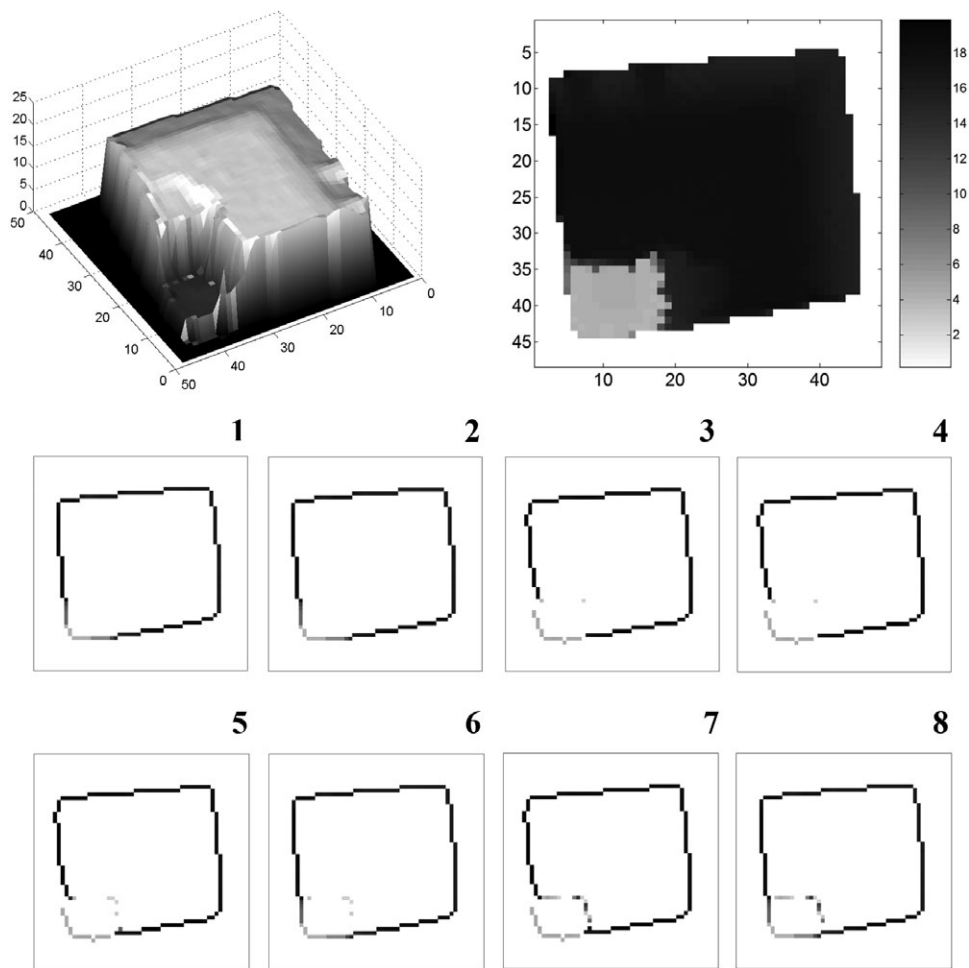


2
3 **Figure 8** Extraction of the volume of a building using the n2.5-DUSM of buildings
4 (enhanced and unenhanced models)

5
6 *3.4.4 The calculation of the morphological indicators: volume of buildings, area*
7 *of roofs, and area of façades*

8
9 **Volume of buildings**

10 The n2.5-DUSM of buildings was used for the calculation of each building's volume. The
11 volume was built from each pixel within a grid size of 0.5 m and was obtained by
12 multiplying the unit square of the pixel itself by the height derived from the correspond-
13 ing intensity value on the n2.5-DUSM of buildings, such as presented in Figure 8. Thus,
14 in order to derive the volume of each building, pixel volumes⁴ overlaying the correspond-
15 ing 2D digital (vectorial) building area were aggregated and summed.



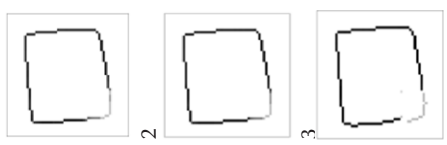
1 **Figure 9** An example of an analyzed object and the detection of edges with eight
2 variations on the procedure

3
4 Area of façades and area of roofs



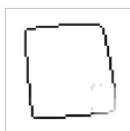


5 Out of this basic procedure eight different variations were created, as shown in Figure 9
6 and explained in Table 1. Several morphological operations on pixels were scrutinized
7 and it was decided to proceed with the fastest techniques, applying small changes in the
8 parameters used. In fact, slight changes in the definition of the parameters of the
9 morphological operations (size and shape of the neighbourhood, filters used in the edge
10 detection) can dramatically affect the results (refer to Figure 10 for some examples of
11 structuring elements used); the use of more sensitive edge detectors allows the identifica-
12 tion of the edges of internal surfaces in the case of complex geometries, as presented in
13 Section 4. For instance, the main issue with morphological indicators is related to the
14 variation of the vertical section of the object. As an example, refer to Figure 11, where
15 the tower does not correspond to the footprint of the basement. These complex shapes

Table 1 Eight variations on the morphological operations used to enhance the edges of vertical surfaces

Case ID	Enhancement on the original DUSM	2 Morphological operation to contract and dilate the perimeter of the object + application of the Canny filter			3 Morphological operation on the enhanced model (point 1) to detect edges applying a diamond filter			Short description of the procedure	
		Description of the applied neighborhood	Size	Shape	Description of the applied neighborhood	Size	Shape		
1	No		3 × 3	Diamond				No	
2	No		5 × 5	Diamond				no	
3	Yes		5 × 5	Diamond		3 × 3	Diamond	5	Yes



1 2 3 4 5 6 7 8 9 10 11 12 13 14 15 16 17 18 19

4		Only for internal facades	5 × 5	Diamond	13	3 × 3	Square	9	Yes	Selecting detected external edges from case 2 and internal ones from case 3
5		Yes	5 × 5	Diamond	13	3 × 3	Square	9	Yes	Selecting detected external edges from case 2 and internal ones from case 3
6		Only for internal facades	5 × 5	Diamond	13	5 × 5	Diamond	13	Yes	Selecting detected external edges from case 2 and internal ones from case 5
7		Yes	5 × 5	Diamond	13	5 × 5	Diamond	13	Yes	Selecting detected external edges from case 2 and internal ones from case 5
8		Only for internal facades	5 × 5	Diamond	13	5 × 5	Diamond	13	Yes	Selecting detected external edges from case 2 and internal ones from case 7

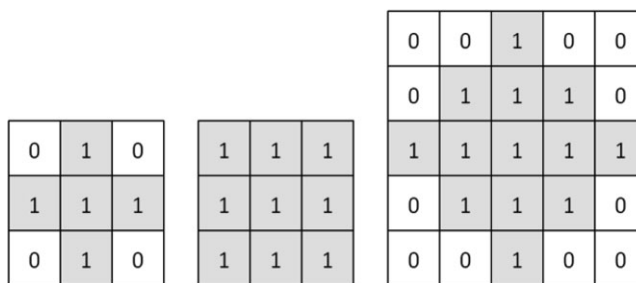


Figure 10 Details of structuring elements used to enhance the model

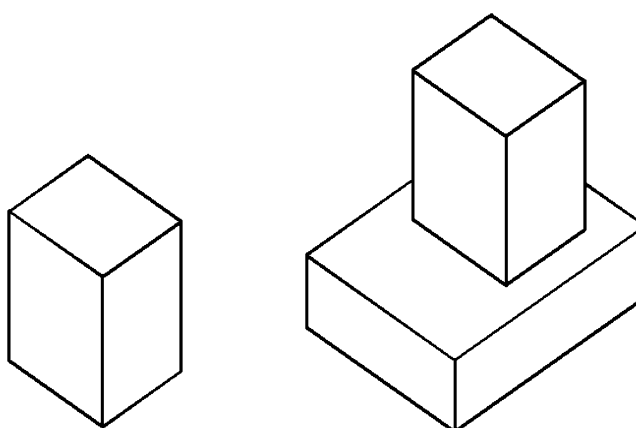


Figure 11 From simple (left) to complex (right) geometry: the tower on a basement

are difficult to analyze, because the external perimeter does not include the edges of the tower. Hence, many edge detectors do not recognize the internal perimeters.

Concerning the proposed eight variations in particular, the external edges of objects can be detected using different neighborhoods for the variations number 1 and 2. In addition, the use of more sensitive edge detectors allows the identification of the boundaries of internal surfaces in the case of complex geometries (variations 3, 5, and 7). Finally, three optimized variations are proposed (variations 4, 6, and 8) where the computation of external edges of case 2 are combined with the computation of internal edges of case 3, 5, and 7.

Once the external and internal edges were detected, the height of the pixel could be derived. Concerning the determination of the length of pixels, it is important to precisely locate those pixels belonging to diagonal segments on the perimeter and assign a longer linear extension. It is not an easy task to define the correct method to calculate the perimeter of an object based on a pixel structure. In order to reduce the error during the computation, it was decided to distinguish only between two lengths to assign to each edge pixel: pixels of value $1*u$ and "diagonal" pixels with value $\sqrt{2}*u$ (where u represents the original unit of the pixel-grid defined on the DUSM). This method is a good compromise for a quick and accurate computation; for instance, methods that use more fine-grained pixel-lengths require the application of larger neighborhoods to detect the

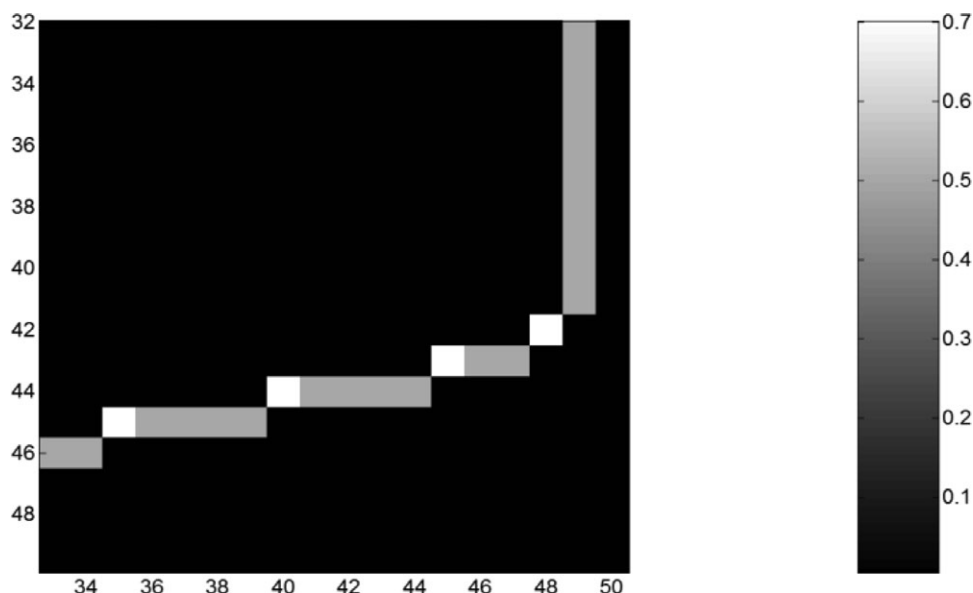


Figure 12 A detail of the edge of an object showing the lengths assigned to each pixel. The unit u of the grid is 0.5 m: pixels have values of $1*u$ and $\sqrt{2}*u$

inclination of the pixel, and this operation often leads to computational mistakes. Hence, it was decided to apply an analysis performed on the sequence of the perimeter segment and simply to assign the $\sqrt{2}*u$ value every time the pixels in the series were only 8-connected but not 4-connected⁵ (refer to Figure 12). Finally, by multiplying the height of each pixel by its length the area of each façade segment could be obtained.

A slightly different procedure can be applied to calculate the areas of roofs. In that case, the surface of the pixel can be calculated once the slope of each pixel is known. For instance, the areas of pixels can vary depending on their inclination. The surface of the pixels can easily be calculated by applying trigonometric formulae. In this work six classes of slopes were distinguished (each class was characterized in steps of 15 degrees, from 0 to 75 degrees). Next the slopes of the pixels were reclassified in order to eliminate those parts that can represent the contours of buildings, i.e. the vertical surfaces. In Figure 13 the reclassification of the slopes on a pixel basis is shown: on the left, the slopes are represented on a pixel basis, whereas on the right slopes higher than 60 degrees are set to 0. Moreover, slopes higher than 45° or 60° were also reclassified using different structuring elements (3 pixels by 3 pixels or 13 diamond pixel filter sizes). The segmentation procedure for laser scanning data was independently implemented to search for planar faces in order to define the slope of each roof section more accurately, when compared to slope automatically calculated using the n2.5-DUSM. Finally, in order to derive the area of each roof, pixel areas⁶ overlaying the corresponding 2D projection of 3D digital (vectorial) roof areas were aggregated and summed.

4 Performed Calculations

The analyses are grouped in two parts, corresponding to the two case-study areas (refer to Table 2). For each site the same three computations were performed, based on the use

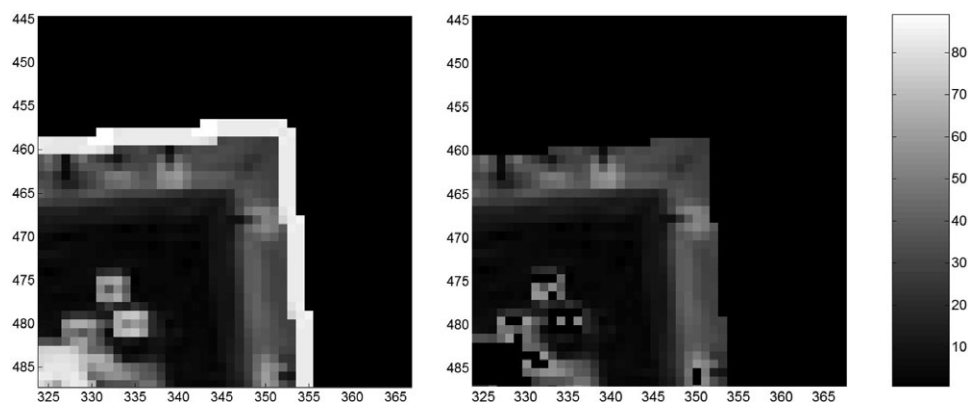


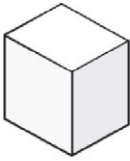
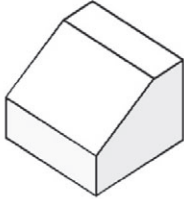
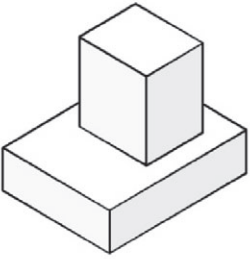
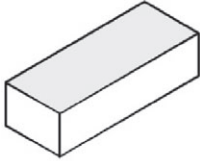
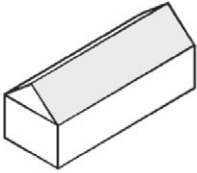
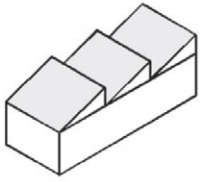
Figure 13 The reclassification of the slopes of the roof pixels. Left, the slopes on a pixel basis, right the slopes higher than 60 degrees are set to 0. In fact, brighter pixels on the edges of the object and features do not appear on the image on the right

Table 2 The sets of analyses conducted on the two case-study areas using different source information

	Number of analyzed buildings
1 Case study at CERN	
1A: Analysis of normalized 2.5-D DUSM derived from building outlines and LiDAR data for volume calculation	10
1B: Analysis of the 2.5-D nDUSM derived from the 2D projection of the 3D model of roof lines and LiDAR data for areas of roofs calculation	10
1C: Analysis of the 2.5-D nDUSM derived from building outlines (also external façades of the 3D model of buildings) and LiDAR data for areas of façades calculation	18
2 Case study in the center of Geneva	
2A: Analysis of the 2.5-D DUSM derived from building outlines and LiDAR data for volume calculation	34
2B: Analysis of the 2.5-D nDUSM derived from the 2D projection of the 3D model of roof lines and LiDAR data for areas of roofs calculation	17
2C: Analysis of the 2.5-D nDUSM derived from building outlines (also external façades of the 3D model of buildings) and LiDAR data for areas of façades calculation	44

of different source information, as follows: (1) building outlines and LiDAR data; (2) 2D projection of the 3D model of roof lines and LiDAR data.

In order to organize the statistical analysis, three possible geometric primitives that describe both roofs and façades are referred to. These categories, represented in Figure 14, are mainly:

	Simple	Intermediate	Multifaceted
Primitives of façades			
	Flat	Classic	Complex
Primitives of roofs			

1 **Figure 14** Different primitives considered for façades and roofs

- 2
- 3 1. The flat roofs and the simple façades: both are defined by flat planes without
- 4 interruptions (e.g. flat roofs).
- 5 2. The classic roofs and the intermediate façades: these are defined by multiple surfaces
- 6 but do not include jumps among its faces (typically continuous pitched roofs).
- 7 3. The complex roofs and the multifaceted façades, whereby different planes determine
- 8 discontinuities among the surfaces (typically shaded roofs or façades in terraced
- 9 buildings).

10

11 **5 Assessment of the Performed Calculations**

12 **5.1 Presentation**

13 The statistical analysis was performed to validate the method. The computed morpho-

14 logical properties (volumes, areas of façades, and areas of roofs) through the different

15 local morphological operations on the n2.5-DUSM of buildings and the n2.5-DUSM of

16 roofs (see Section 4) were compared to the outputs directly calculated using the 3D

17 vectorial city model.

18 Results summarized in Tables A1–A10 of the Appendix are grouped by morpho-

19 logical property, distinguishing between: (a) the global (all buildings) and the building by

Table 3 Hypothesis related to the significance tests conducted in this study

	Significance statistical analysis (<i>t</i> test; level of significance: 0.05)	
	Null Hypothesis (H_0)	Hypothesis 1 (H_1)
Test 1	No significant improvement	Significant improvement
For volumes, areas of roofs and areas of façades	between the use of the unenhanced and the enhanced models for the calculation of volumes, areas of roofs and areas of façades	between the use of the unenhanced and the enhanced models for the calculation of volumes, areas of roofs and areas of façades
Test 2	No significant improvement	Significant improvement
Only for areas of façades	between the use of the unenhanced and the optimized models for the calculation of areas of façades	between the use of the unenhanced and the optimized models for the calculation of areas of façades
Test 3	No significant improvement	Significant improvement
Only for areas of roofs	between the use of the unenhanced model and the segmentation technique for the calculation of areas of roofs	between the use of the unenhanced model and the segmentation technique for the calculation of areas of roofs

building analysis; (b) the use of the unenhanced, enhanced, and optimized models and the segmentation procedure; (c) the level of complexity of building and roof types (see Figure 14).

In particular, the “global deviation error” is defined as the relation of the global (all buildings) calculated morphological indicator derived from LiDAR data and the theoretical known value, whereas the “absolute building deviation error” for each building represents the absolute relation of the calculated morphological indicator derived from LiDAR data and the theoretical known value.

Moreover, a two-tailed “*t*-test” significance statistical analysis was applied to each of the morphological properties of buildings calculated using the unenhanced, the enhanced, and the optimized 2.5-DUSM models and the segmentation procedure. This test allows the interpretation of the probability related to the decreasing of the absolute deviation error between each pair of buildings of the following cases: (a) the unenhanced and the enhanced models; (b) the unenhanced model and the segmentation procedure; (c) the unenhanced and the optimized models.

The reason to have applied a two-tailed “*t*-test” and not a simpler one-tailed “*t*-test” is that differences between each pair of buildings can be positive or negative, guaranteeing a more strict significance statistical test. Thus, for each of the three morphological properties of the evaluated buildings, the null hypothesis H_0 was tested as shown in Table 3.

Table 4 Significance statistical analysis on volumes to test the improvement of the proposed calculation, referring to different types of considered buildings in the enhanced and unenhanced models

CERN + Centre of Geneva
 Volumes of roofs
 Significance statistical analysis (*t* test; level of significance: 0.05)

Volumes of 44 buildings (complex, classic and flat roofs)	Test 1 Enhanced Model	Volumes of 21 buildings (classic only)	Test 1 Enhanced Model
Unenhanced Model	0.14 <i>Significance of improvement: No</i>	Unenhanced Model	0.13 <i>Significance of improvement: No</i>
Volumes of 10 buildings (complex only)	Test 1 Enhanced Model	Volumes of 13 buildings (flat only)	Test 1 Enhanced Model
Unenhanced Model	0.49 <i>Significance of improvement: No</i>	Unenhanced Model	0.59 <i>Significance of improvement: No</i>

The significance level (α) was set to 0.05, which means that H_0 was rejected in favor of H_1 when α was lower than 0.05. For more details about the significance tests calculated for each of the morphological properties of buildings under analysis please consult Tables 4–6.

5.2 Output Results for Volumes and Discussion

In general, as was stated at the beginning of this article, it is easy to derive volumes using DIP techniques and this work does not propose significant improvements to the traditional pixel based computation.

In particular, the analysis summarized in Tables A1 and A2 of the Appendix shows that no major improvement can be reached using the enhanced model to reduce the global deviation error, even if at the building's scale (Table A2) some minor, non-significant improvement is noticed for the absolute building deviation error. This happens because in the process of enhancement on the perimeter the distribution of intensity values inside the neighborhood is averaged, thus reducing the effects of LiDAR interpolation and obtaining more defined edges. This enhancement does not really affect the overall volume calculation, but it has a significant effect on the calculation of the façade areas. Moreover, results of deviation show that volumes are always slightly overestimated for both the enhanced and the unenhanced models.

The significance statistical analysis that tests the improvement of using the unenhanced model versus the enhanced model for the calculation of volumes is shown in Table 4, confirming that no significant improvements were achieved for the different types of considered buildings.

Table 5 Significance statistical analysis on the areas of façades to test the improvement of the proposed calculation, referring to different types of considered buildings in the enhanced (case 7) and optimized models (case 8)

CERN + Centre of Geneva
Areas of façades
Significance statistical analysis (*t* test; level of significance: 0.05)

<i>Areas of façades of 62 buildings (multifaceted, intermediate and simple buildings)</i>	Test 1 Enhanced Model (case 7)	Test 2 Optimized Model (case 8)
Unenhanced Model (case 1)	0.095 <i>Significance of improvement:</i> No	1E-3 <i>Significance of improvement:</i> Yes
<i>Areas of façades of 18 multifaceted buildings</i>	Test 1 Enhanced Model (case 7)	Test 2 Optimized Model (case 8)
Unenhanced Model (case 1)	3E-04 <i>Significance of improvement:</i> Yes	1E-3 <i>Significance of improvement:</i> Yes
<i>Areas of façades of 30 intermediate buildings</i>	Test 1 Enhanced Model (case 7)	Test 2 Optimized Model (case 8)
Unenhanced Model (case 1)	0.14 <i>Significance of improvement:</i> No	0.47 <i>Significance of improvement:</i> No
<i>Areas of façades of 14 simple buildings</i>	Test 1 Enhanced Model (case 7)	Test 2 Optimized Model (case 8)
Unenhanced Model (case 1)	0.54 <i>Significance of improvement:</i> No	0.25 <i>Significance of improvement:</i> No

5.3 Output Results for the Areas of Façades and Discussion

In this analysis (Tables A3 and A4 of the Appendix) the accuracy of the eight proposed variations (see, for instance, Table 1) for the calculation of the areas of façades was assessed.

Referring to the validation of the computation of the areas of façades, it can be seen that among the proposed variations of the procedure to enhance the model (refer to Section 3.4.4) the variation number 7 gives the best results at a global level. If the precision at the building level is analyzed, variation number 8 performs better. The reason is that for these particular routines larger neighborhoods were used to enhance the edges of the object, thus enabling the detection of more internal vertical surfaces. This makes the difference, mainly in the case of multifaceted buildings, such as towers on the basement, as shown in Figure 11.

Table 6 Significance statistical analysis on roof areas to test the improvement of the proposed calculation, referring to different types of considered buildings in the enhanced and unenhanced models and the segmentation procedure

CERN + Centre of Geneva
 Areas of roofs
 Significance statistical analysis (*t* test; level of significance: 0.05)

Areas of all roofs (27 buildings)	Test 1 Enhanced Model (reclassification of slopes > 45° to 0°)	Test 1 Enhanced Model (reclassification of slopes > 45°) by applying a 13 size diamond mask	Test 3 Segmentation procedure
Unenhanced Model (not reclassified)	1E-05 <i>Significance of improvement: Yes</i>	1E-05 <i>Significance of improvement: Yes</i>	2E-05 <i>Significance of improvement: Yes</i>
Areas of complex roofs (15 buildings)	Test 1 Enhanced Model (reclassification of slopes > 45° to 0°)	Test 1 Enhanced Model (reclassification of slopes > 45°) by applying a 13 size diamond mask	Test 3 Segmentation procedure
Unenhanced Model (not reclassified)	1E-03 <i>Significance of improvement: Yes</i>	1E-03 <i>Significance of improvement: Yes</i>	9E-04 <i>Significance of improvement: Yes</i>
Areas of classic roofs (6 buildings)	Test 1 Enhanced Model (reclassification of slopes > 45° to 0°)	Test 1 Enhanced Model (reclassification of slopes > 45°) by applying a 13 size diamond mask	Test 3 Segmentation procedure
Unenhanced Model (not reclassified)	0.041 <i>Significance of improvement: Yes</i>	0.045 <i>Significance of improvement: Yes</i>	0.040 <i>Significance of improvement: Yes</i>
Areas of flat roofs (6 buildings)	Test 1 Enhanced Model (reclassification of slopes > 45° to 0°)	Test 1 Enhanced Model (reclassification of slopes > 45°) by applying a 13 size diamond mask	Test 3 Segmentation procedure
Unenhanced Model (not reclassified)	0.037 <i>Significance of improvement: Yes</i>	0.039 <i>Significance of improvement: Yes</i>	0.034 <i>Significance of improvement: Yes</i>

1 The significance statistical analysis that tests the improvement of using the unen-
2 hanced model versus the enhanced model (case 7) and the unenhanced model versus the
3 optimized model (case 8) shows a significant improvement for the calculation of areas of
4 façades of multifaceted buildings in both cases. Moreover, the significance statistical
5 analysis shows that the optimized model (case 8) also presents a significant improvement
6 when evaluating all three types of buildings in a single dataset. For more details please
7 consult Table 5.

8 9 *5.4 Output Results for the Areas of Roofs and Discussion*

10 In this set of analyses (Tables A5 to A10 of the appendix), both methods (DIP techniques
11 and segmentation of planar areas) were processed on the unenhanced and enhanced
12 models.

13 Concerning the segmentation procedure applied for areas of façades calculation, it
14 was noticed that many superstructures on roofs – especially in the Geneva city center
15 case-study area – were not easy to detect. For instance, buildings with classic and
16 complex geometries having many superstructures on roofs caused lower accuracies and
17 higher standard deviations. The reclassification (for more details refer to Section 3.4.4)
18 with DIP techniques of those pixels having slopes higher than 45 or 60 degrees proved
19 to be a good alternative for the segmentation procedure. In fact, this is particularly
20 important in the case where 3D roof prints are not available, even if the 2D outlines of
21 building footprints do not always represent the outline of the building roof.

22 The significance statistical analysis that tests the improvement of using: (1) the
23 unenhanced model versus the enhanced model by reclassifying slopes $> 45^\circ$ to 0° ; (2) the
24 unenhanced model versus the enhanced model with reclassification of slopes $> 45^\circ$ by
25 applying a 13 size diamond mask; and (3) the unenhanced model versus the segmentation
26 procedure, shows a significant improvement for all cases, as presented in Table 6.

27 28 *5.5 General Remarks on the Results*

29 The results shown in the tables of the Appendix, complemented by the significance
30 statistical analysis presented in Sections 5.2–5.4, demonstrate that the methods proposed
31 here can reach higher levels of accuracy by reducing the global and absolute building
32 deviation errors to the real 3D vectorial city model. The best results achieved from all the
33 techniques and models used are summarized in Table 7.

34 Finally, some general remarks are presented concerning the results achieved consid-
35 ering the significance statistical analysis:

- 36 • For the analysis of volumes, the use of the enhanced model is not justified. In fact, the
37 global analysis with the unenhanced model performs better, since the procedure of
38 enhancement tends to overweight the intensity values of pixels.
- 39 • The enhanced model is particularly suitable to improve results for the calculation of
40 façade and roof areas.
- 41 • The segmentation procedure performs better for the analysis of roof areas, even if the
42 use of DIP for reclassification of slopes higher of 45° by applying a 13 diamond filter
43 is a good alternative when the segmentation procedure is not applied to raw LiDAR
44 data.
- 45 • The optimized model is a good option for the calculation of façade areas, especially
46 for zones characterized by low density built-up areas with simple buildings.

Table 7 Review of best results achieved by applying the proposed methods

CERN + Centre of Geneva Volumes			
	Global Analysis (Unenhanced Model)	Building by Building analysis (Enhanced Model)	
Type of building	Global deviation error	Absolute building deviation error	Standard deviation
Total	2.30%	4.09%	3.26%
Simple	3.82%	4.15%	3.30%
Intermediate	0.99%	4.25%	2.93%
Multifaceted	0.90%	5.49%	4.40%

CERN + Centre of Geneva Areas of facades			
	Global Analysis (Enhanced Model: case 7)	Building by Building analysis (Optimized Model: case 8)	
Type of building	Global deviation error	Absolute building deviation error	Standard deviation
Total	-3.45%	6.78%	6.77%
Simple	-5.03%	5.04%	2.80%
Intermediate	3.53%	4.07%	4.15%
Multifaceted	-9.78%	10.92%	7.32%

CERN + Centre of Geneva Areas of roofs			
	Global Analysis (Segmentation Technique)	Building by building analysis (Segmentation Technique)	
Type of building	Global deviation error	Absolute building deviation error	Standard deviation
Total	1.19%	3.47%	4.09%
Simple	-1.57%	1.19%	0.59%
Intermediate	-0.95%	2.79%	3.43%
Multifaceted	1.74%	4.45%	4.71%

6 Conclusions and Future Work

This work presents a method to calculate the morphological properties of the built environment using LiDAR data, GIS data and 3D models of cities through segmentation and image processing techniques. The developed procedure is intended to fill the gap in this sector, thus enabling the use of LiDAR data for numerous applications at the level of the urban fabric. Using different techniques to reconstruct and analyze the model, we calculated morphological properties of the built fabric. Afterwards, the outputs were then validated through a comparison to the 3D vectorial city model. The conducted analysis on two case-study areas, characterized by very different geometries of buildings, allows the conclusion that the methods can be extended on other cases. For instance, the calculation procedure should be chosen according on the complexity of the urban fabric.

Once the areas of the surfaces and the built volumes are assessed, other minor indicators can be easily derived with DIP techniques (pixel analysis):

- General morphological indicators: the total built floor area considering all storeys (mean storey height is assumed to be 3 m); the mean height of buildings on the site.
- Derived indicators of density: urban density, as follows: the built volume on the considered urban area (m^3/m^2); the ground occupation index, i.e. the covered area to the urban area ratio (m^2/m^2); the floor area ratio (FAR) (m^2/m^2).

This short list of derived indicators demonstrates how significant it is to accurately compute the urban surfaces, if we want to use this type of information for helpful applications in urban studies, in particular in the field of the UEQ and the assessment of energy consumption of the built fabric. In fact, as presented above in Section 2, calculations of solar radiation exchange, energy demand, and visibility analysis require a reliable dimensioning of the urban surfaces.

For instance, the proposed n2.5-DUSMs derived from LiDAR data include all the features, like roof superstructures, that are crucial in the estimation of solar radiation and are generally ignored by most of the existing 3D models. Moreover, n2.5-DUSMs derived from LiDAR surveys could also take vegetation into account, thus providing a quantification of natural elements (vegetation density).

Future work will focus on the following aspects to improve the method:

- To automate the process to directly calculate the morphological properties from the raw LiDAR data. This step requires the implementation of new software that includes the potential of all software that was used in this work.
- To improve some minor issues concerning complex buildings, for example refining the computation of superstructures on roofs.
- To consider carefully those parts of the built environment that are strongly limited by vegetation (e.g. big portions of trees covering the roofs) during the phase of reconstruction of the model.
- To test the robustness of the methods presented here by evaluating their sensitivity to the variation of grid size and to the discrepancy of sampling density of raw LiDAR point datasets.

Finally, taking into account the technologies that are currently under rapid development, it is very plausible that in the near future the extraction of morphological properties of buildings could also happen through computer vision oriented photogrammetry that is yielding innovative approaches for the automatic reconstruction and interpretation of

1 building façades. In any case, since the aim of this work is to provide a fast but accurate
2 computation at the district and urban level, the prospect of including photogrammetry
3 into the proposed method still seems to be remote, due to the heavy data analysis
4 involved.

6 Endnotes

- 8 1 For both case-study areas, external facades (outlines) of buildings were defined using the
9 existing 2D GIS cadastral information, which means that n2.5-DUSM of buildings can also be
10 also applied for the calculation of areas of facades, such as presented in Section 3.4.4.
- 11 2 The Canny filter is considered as the most powerful edge detection method. It identifies strong
12 and weak edges and its peculiarity is that it takes weak edges only into consideration when they
13 are connected to strong ones. This allows a reduction in noise in the image.
- 14 3 Flat structuring elements can vary according to their size (neighborhood) and their shape. The
15 neighborhood is a matrix containing 1s (the so-called neighbors) and 0s. The location of the 1s
16 defines the neighborhood for the morphological operation. In the routine the neighborhood is
17 centered on those pixels on which image enhancement is to be applied (in this case the pixels on
18 the perimeter of the object). Beside the definition of the neighborhood as the size of the filter, the
19 shape of the filter itself has also to be established, in other words where the 1s are disposed
20 inside the neighborhood.
- 21 4 The total volume built for each building comes straightforwardly by adding the elementary
22 volumes of its pixels.
- 23 5 The term “adjacency” is used in image processing to define “connected components,” also
24 referred as “objects.” Pixels can be primarily 4-connected or 8-connected, depending on the
25 definition of adjacency. Generally, 4-connected pixels do not count diagonal neighbors, whereas
26 8-connected do (Gonzalez et al. 2009).
- 27 6 The total area of each roof comes straightforwardly by adding the elementary areas of its pixels.

29 References

- 31 Aalders H 2002 The registration of quality in a GIS. In Shi W, Fisher P F, and Goodchild M F (eds)
32 *Spatial Data Quality*. London, Taylor and Francis: 186–99
- 33 Behan A 2000 On the matching accuracy of rasterised scanning laser altimeter data. *International*
34 *Archives of Photogrammetry, Remote Sensing and Spatial Information Sciences* 33(B2):
35 75–82
- 36 Canny J 1986 A computational approach to edge detection. *IEEE Transactions Pattern Analysis*
37 *and Machine Intelligence* 8: 679–714
- 38 Carneiro C, Karzand M, Golay F, Lu Y M, and Vetterli M 2010 Assessing digital surface models
39 by verifying shadows: a sensor network approach. In Devillers R and Goodchild H (eds)
40 *Spatial Data Quality: From Process to Decisions*. Boca Raton, CRC Press: 147–61
- 41 Carneiro C, Morello E, and Desthieux G 2009a Assessment of solar irradiance on the urban fabric
42 for the production of renewable energy using LIDAR data and image processing techniques. In
43 Sester M, Bernard L, and Paelke V (eds) *Advances in Giscience, Lecture Notes in Geoinfor-*
44 *mation and Cartography*. Berlin, Springer: 83–110
- 45 Carneiro C, Morello E, Ratti C, and Golay F 2008 Solar radiation over the urban texture: LIDAR
46 data and image processing techniques for environmental analysis at city scale. In Lee J and
47 Zlatanova S (eds) *3-D Geo-Information Sciences, Lecture Notes in Geoinformation and*
48 *Cartography*. Berlin, Springer: 319–40
- 49 Carneiro C, Silva V, and Golay F 2009b Incorporation of morphological properties of buildings’
50 descriptors computed from GIS and LIDAR data on an urban multiagent vector based
51 geosimulator. In Gervasi O, Taniar D, and Murgante B (eds) *Lecture Notes in Computer*
52 *Science: Computational Science and Its Applications*. Berlin, Springer: 205–20

- 1 Devillers R, Bedard Y, and Jeansoulin R 2005 Multidimensional management of geospatial data
2 quality information for its dynamic use within GIS. *Photogrammetric Engineering & Remote*
3 *Sensing* 71(2): 205–15
- 4 Gonzalez R C, Woods R E, and Eddins S L 2009 *Digital Image Processing Using Matlab*. Knoxville,
5 TN, Gatesmark Publishing
- 6 Haala N, Brenner C, and Anders K-H 1998 3D urban GIS from laser altimeter and 2D map data.
7 *International Archives of Photogrammetry, Remote Sensing and Spatial Information Sciences*
8 32(3/1): 339–46
- 9 Hofmann A, Maas H-G, and Streilein A 2003 Derivation of roof types by cluster analysis in
10 parameter spaces of airborne laserscanner point clouds. *International Archives of Photogram-*
11 *metry, Remote Sensing and Spatial Information Sciences* 34(3/W13): 112–17
- 12 Koomen E and Bação F 2005 Searching for the polycentric city: a spatio-temporal analysis of Dutch
13 urban morphology. In AGILE (ed) *Proceedings of the 8th AGILE Conference on GIS*, 26–8
14 May, Lisbon, Portugal
- 15 Lemp D and Weidner U 2005 Improvements of roof surface classification using hyperspectral and
16 laser scanning data. *International Archives of Photogrammetry, Remote Sensing and Spatial*
17 *Information Sciences* 36(8/W27): ●●●●
- 18 Morello E and Ratti C 2009a SunScapes: “solar envelopes” and the analysis of urban DEMs. [2]
19 *Computers, Environment and Urban Systems* 33: 26–34
- 20 Morello E and Ratti C 2009b A digital image of the city: 3-D isovists in Lynch’s Urban Analysis.
21 *Environment and Planning B: Planning and Design* 36: 837–53
- 22 Osaragi T and Otani I 2007 Effects of ground surface relief in 3-D spatial analysis on residential
23 environment. In Fabrikant S and Wachowicz M (eds) *The European Information Society:*
24 *Lecture Notes in Geoinformation and Cartography*. Berlin, Springer: 171–86
- 25 Quint F and Landes S 1996 Colour aerial image segmentation using a Bayesian homogeneity
26 predicate and map knowledge. *International Archives of Photogrammetry, Remote Sensing*
27 *and Spatial Information Sciences* 31(B3): 663–8
- 28 Ratti C and Richens P 2004 Raster analysis of urban form. *Environment and Planning B: Planning*
29 *and Design* 31: 297–309
- 30 Rottensteiner F, Trinder J, Clode S, and Kubik K 2005 Automated delineation of roof planes from
31 LIDAR data. In Vosselman G and Brenner C (eds) *Proceedings of the ISPRS Workshop Laser*
32 *Scanning 2005. ISPRS Workshop Laser Scanning 2005*. Enschede, The Netherlands, Septem-
33 ber 12–14 221–26
- 34 Voegtle T and Steinle E 2000 3-D modelling of buildings using laser scanning and spectral infor-
35 mation. *International Archives of Photogrammetry, Remote Sensing and Spatial Information*
36 *Sciences* 33(B3): 927–34
- 37 Vosselmann G 2002 Fusion of laser scanning data, maps and aerial photographs for building
38 reconstruction. In IEEE (ed) *Proceedings of the International Geoscience and Remote Sensing*
39 *Symposium*. Toronto, Canada, June 24–28: 85–8
- 40 Vosselmann G and Dijkman S 2001 3-D building model reconstruction from point clouds and
41 ground plans. *International Archives of Photogrammetry, Remote Sensing and Spatial Infor-*
42 *mation Sciences* 34(3/W4): 37–44
- 43 Yoshida H and Omae M 2005 An approach for analysis of urban morphology: methods to derive
44 morphological properties of city blocks by using an urban landscape model and their inter-
45 pretations. *Computers, Environment and Urban Systems* 29: 223–47
- 46 Zinger S, Nikolova M, Roux M, and Maître H 2002 3D resampling for airborne laser data of urban
47 areas. *International Archives of Photogrammetry, Remote Sensing and Spatial Information*
48 *Sciences* 34(3B): 55–61

Appendix
Table A1 Global analysis of volumes using DIP techniques. Left-hand side: unenhanced model; right-hand side: enhanced model

CERN + Center of Geneva		Global volume analysis unenhanced n2.5-DUSM				Global volume analysis enhanced n2.5-DUSM			
Type of building	Volume DIP techniques [m ³]	Volume 3-D model [m ³]	Global deviation error	Type of building	Volume DIP techniques [m ³]	Volume 3-D model [m ³]	Global deviation error	Type of building	Volume 3-D model [m ³]
Total	345,887.50	338,114.86	2.30%	Total	346,105.48	338,114.86	2.36%	Total	338,114.86
Simple	164,666.78	158,603.22	3.82%	Simple	164,144.23	158,603.22	3.49%	Simple	158,603.22
Intermediate	108,754.36	107,689.42	0.99%	Intermediate	108,734.80	107,689.42	0.97%	Intermediate	107,689.42
Multifaceted	72,466.35	71,822.22	0.90%	Multifaceted	73,226.44	71,822.22	1.96%	Multifaceted	71,822.22

Table A2 Building by building analysis of volumes using DIP techniques. Left-hand side: unenhanced model; right-hand side: enhanced model

CERN + Center of Geneva		Building by building analysis unenhanced n2.5-DUSM		Building by building analysis enhanced n2.5-DUSM	
Type of building	Volume [m ³] Absolute building deviation error	Volume [m ³] Standard deviation	Type of building	Volume [m ³] Absolute building deviation error	Volume [m ³] Standard deviation
Total	4.61%	3.16%	Total	4.09%	3.26%
Simple	3.55%	2.03%	Simple	4.15%	3.30%
Intermediate	4.82%	3.74%	Intermediate	4.25%	2.93%
Multifaceted	6.15%	2.96%	Multifaceted	5.49%	4.40%

1
2
3
4
5
6
7
8
9
10
11

Table A3 Global analysis of façade areas using DIP techniques; se, structural element; EM, enhanced model; OM, optimized model

CERN + Center of Geneva		Area case 1 (se1) [m ²]	Area case 2 (se2) [m ²]	Area case 3 (EM) [m ²]	Area case 4 (OM) [m ²]	Area case 5 (EM, se9) [m ²]	Area case 6 (OM, se9) [m ²]	Area case 7 (EM, se13) [m ²]	Area case 8 (OM, se13) [m ²]
Type of building	Area 3-D model [m ²]								
Global area analysis									
Total	101,932.72	90,431.09	93,182.06	93,783.39	93,658.76	96,079.59	94,414.16	98,412.25	95,771.98
Simple	25,101.98	22,387.44	22,943.92	23,157.69	23,092.32	23,397.91	23,178.98	23,839.17	23,344.06
Intermediate	31,590.72	31,095.59	31,893.52	31,890.47	31,960.82	32,333.79	32,002.02	32,706.58	32,133.42
Multifaceted	45,240.02	35,918.56	37,304.22	37,694.93	37,565.22	39,303.39	38,192.76	40,815.50	39,254.10
Global deviation error									
Total	-	-11.28%	-8.58%	-7.99%	-8.12%	-5.74%	-7.38%	-3.45%	-6.04%
Simple	-	-10.81%	-8.60%	-7.75%	-8.01%	-6.79%	-7.66%	-5.03%	-7.00%
Intermediate	-	-1.57%	0.96%	0.95%	1.17%	2.35%	1.30%	3.53%	1.72%
Multifaceted	-	-20.60%	-17.54%	-16.68%	-16.96%	-13.12%	-15.58%	-9.78%	-13.23%

Table A4 Building by building analysis of façade areas using DIP techniques; se, structural element; EM, enhanced model; OM, optimized model

CERN + Center of Geneva		area case 1 (se1) [m ²]	area case 2 (se2) [m ²]	area case 3 (EM) [m ²]	area case 4 (OM) [m ²]	area case 5 (EM, se9) [m ²]	area case 6 (OM, se9) [m ²]	area case 7 (EM, se13) [m ²]	area case 8 (OM, se13) [m ²]
Type of building									
Building by building analysis: absolute building deviation error									
Total		9.46%	8.38%	8.85%	8.01%	8.12%	7.38%	7.66%	6.78%
Simple		6.46%	6.00%	6.15%	5.63%	5.78%	5.39%	5.12%	5.04%
Intermediate		4.52%	4.06%	4.53%	4.08%	5.37%	4.06%	5.90%	4.07%
Multifaceted		17.24%	14.88%	15.62%	14.02%	12.36%	12.32%	10.85%	10.92%
Building by building analysis: standard deviation									
Total		9.95%	9.14%	9.33%	8.70%	7.53%	7.76%	6.82%	6.77%
Simple		5.53%	4.51%	3.65%	3.62%	3.63%	3.29%	4.10%	2.80%
Intermediate		3.28%	4.01%	4.67%	4.07%	5.16%	4.11%	5.67%	4.15%
Multifaceted		8.96%	8.42%	8.58%	8.58%	6.14%	7.86%	6.05%	7.32%

Table A5 Global analysis of roof areas using DIP techniques on the unenhanced model

CERN + Center of Geneva		DIP technique: reclassification of image pixel on the unenhanced n2.5-DUSM						
Type of roof	Area 3-D model [m ²]	Area all slopes [m ²]	Area slopes > 15° set to 0° [m ²]	Area slopes > 30° set to 0° [m ²]	Area slopes > 45° set to 0° [m ²]	Area slopes > 60° set to 0° [m ²]	Area slopes > 75° set to 0° [m ²]	
Global area analysis								
Total	35,982.54	49,584.42	34,842.73	35,270.39	36,774.25	37,410.43	41,089.20	
Flat	3,667.58	5,972.75	3,732.15	3,755.51	3,843.22	3,921.60	4,358.22	
Classic	2,608.27	3,190.40	2,457.18	2,592.92	2,666.61	2,680.01	2,787.94	
Complex	29,706.69	4,0421.27	28,653.41	28,921.96	30,264.42	30,808.81	33,943.05	
Global deviation error								
Total	-	37.80%	-3.17%	-1.98%	2.20%	3.97%	14.19%	
Flat	-	62.85%	1.76%	2.40%	4.79%	6.93%	18.83%	
Classic	-	22.32%	-5.79%	-0.59%	2.24%	2.75%	6.89%	
Complex	-	36.07%	-3.55%	-2.64%	1.88%	3.71%	14.26%	

Table A6 Global analysis of roof areas using DIP techniques on the enhanced model

CERN + Center of Geneva		DIP technique: reclassification of image pixel on the enhanced n2.5-DUSM									
Type of roof	Area all slopes [m ²]	Area slopes > 0° set to 0° [m ²]	Area slopes > 15° set to 0° [m ²]	Area slopes > 30° set to 0° [m ²]	Area slopes > 45° set to 0° [m ²]	Area slopes > 60° set to 0° [m ²]	Area slopes > 75° set to 0° [m ²]	Area slopes > 45° using a se diamond 9 [m ²]	Area slopes > 45° using a se diamond 13 [m ²]	Area slopes > 60° using a se diamond 9 [m ²]	Area slopes > 60° using a se diamond 13 [m ²]
Global area analysis											
Total	35,982.54	42,353.39	34,834.97	35,238.59	35,926.27	36,911.09	38,704.25	36,452.85	36,354.15	37,480.13	37,273.57
Flat	3,667.58	4,495.25	3,731.53	3,750.43	3,802.47	3,915.65	4,179.21	3,848.25	3,838.48	3,992.55	3,964.77
Classic	2,608.27	2,973.36	2,453.06	2,569.18	2,591.49	2,615.01	2,640.47	2,610.79	2,609.06	2,629.95	2,624.01
Complex	29,706.69	34,884.78	28,650.39	28,918.98	29,532.32	30,380.43	31,884.57	29,993.81	29,906.61	30,857.63	30,684.79
Global deviation error											
Total	-	17.71%	-3.19%	-2.07%	-0.16%	2.58%	7.56%	1.31%	1.03%	4.16%	3.59%
Flat	-	22.57%	1.74%	2.26%	3.68%	6.76%	13.95%	4.93%	4.66%	8.86%	8.10%
Classic	-	14.00%	-5.95%	-1.50%	-0.64%	0.26%	1.23%	0.10%	0.03%	0.83%	0.60%
Complex	-	17.43%	-3.56%	-2.65%	-0.59%	2.27%	7.33%	0.97%	0.67%	3.87%	3.29%

Table A7 Global analysis of roof areas using the segmentation procedure

CERN + Center of Geneva Segmentation procedure Global area analysis

Type of roof	Area image segmentation technique [m ²]	Area 3D model [m ²]	Global deviation error
Total	35,533.95	35,957.52	1.19%
Flat	3,725.94	3,667.58	-1.57%
Classic	2,633.29	2,608.27	-0.95%
Complex	29,174.72	29,681.67	1.74%

Table A8 Building by building analysis of roof areas using DIP techniques on the unenhanced model

CERN + Center of Geneva

DIP technique: reclassification of image pixel on the unenhanced n2.5-DUSM

Type of roof	Area all slopes [m ²]	Area slopes > 15° set to 0° [m ²]	Area slopes > 30° set to 0° [m ²]	Area slopes > 45° set to 0° [m ²]	Area slopes > 60° set to 0° [m ²]	Area slopes > 75° set to 0° [m ²]
Building by Building analysis: absolute building deviation error						
Total	38.84%	7.51%	6.12%	6.20%	6.26%	13.16%
Flat	38.92%	2.27%	2.93%	8.30%	9.20%	17.71%
Classic	21.76%	5.95%	1.27%	2.26%	2.92%	6.72%
Complex	45.65%	9.89%	9.13%	7.08%	6.62%	14.22%
Total	32.32%	7.80%	7.82%	6.38%	4.74%	9.84%
Flat	34.26%	0.81%	0.92%	5.97%	5.51%	4.99%
Classic	24.59%	2.31%	1.82%	1.46%	1.42%	4.89%
Complex	33.75%	9.46%	9.19%	7.27%	4.77%	11.44%

Table A9 Building by building analysis of roof areas using DIP techniques on the enhanced model

CERN + Center of Geneva		DIP technique: reclassification of image pixel on the enhanced n2.5-DUSM		Area slopes > 75° to 0°		Area slopes > 45° using a se diamond 9		Area slopes > 45° using a se diamond 13		Area slopes > 60° using a se diamond 9		Area slopes > 60° using a se diamond 13	
Type of roof	[m ²]	Area slopes > 15° set to 0°	[m ²]	Area slopes > 30° set to 0°	[m ²]	Area slopes > 45° set to 0°	[m ²]	Area slopes > 45° set to 0°	[m ²]	Area slopes > 60° set to 0°	[m ²]	Area slopes > 60° set to 0°	[m ²]
Total	20.30%	7.44%	6.14%	4.84%	5.49%	7.32%	4.85%	4.80%	5.86%	4.80%	5.86%	4.80%	5.63%
Flat	14.17%	1.80%	2.13%	2.98%	4.90%	9.08%	4.16%	4.00%	6.46%	4.00%	6.46%	4.00%	6.07%
Classic	15.00%	7.08%	1.78%	0.41%	1.35%	2.89%	0.97%	0.78%	2.26%	0.78%	2.26%	0.78%	2.24%
Complex	24.19%	9.71%	9.00%	6.90%	7.22%	8.61%	6.52%	6.46%	7.14%	6.46%	7.14%	6.46%	6.86%
Building by Building analysis: absolute building deviation error													
Total	22.73%	7.67%	7.57%	5.96%	4.50%	6.95%	4.45%	4.65%	4.65%	4.65%	4.65%	4.65%	4.32%
Flat	13.84%	0.70%	0.65%	0.97%	2.88%	7.28%	1.23%	1.06%	3.72%	1.06%	3.72%	1.06%	3.25%
Classic	24.04%	1.16%	2.14%	0.17%	2.17%	5.31%	0.89%	0.85%	2.93%	0.85%	2.93%	0.85%	2.69%
Complex	24.73%	9.14%	8.76%	7.02%	4.68%	7.15%	4.95%	5.31%	4.78%	5.31%	4.78%	5.31%	4.48%
Building by Building analysis: standard deviation													

Table A10 Building by building analysis of roof areas using the segmentation procedure

CERN + Center of Geneva
Segmentation procedure Building by building analysis

Type of roof	Area [m ²] Absolute building deviation error
Total	3.47%
Flat	1.19%
Classic	2.79%
Complex	4.45%

Type of roof	Area [m ²] Standard deviation
Total	4.09%
Flat	0.59%
Classic	3.43%
Complex	4.71%

Toppan Best-set Premedia Limited	
Journal Code: TGIS	Proofreader: Elsie
Article No: 1218	Delivery date: 23 August 2010
Page Extent: 35	

AUTHOR QUERY FORM

Dear Author,

During the preparation of your manuscript for publication, the questions listed below have arisen. Please attend to these matters and return this form with your proof.

Many thanks for your assistance.

Query References	Query	Remark
1	AUTHOR: Carneiro, Karzand, Golay, Lu, Vetterli, 2010 has not been cited in the text. Please indicate where it should be cited; or delete from the Reference List.	
2	AUTHOR: Please provide the page range for Lemp and Weidner 2005.	
3	AUTHOR: Please note that originally Table ID and citations of Tables 8–17 have been changed to Tables A1–A10 as they are in the appendix. Please confirm that it is OK.	